



1

2 **Assessment of shallow landslide susceptibility using an artificial**
3 **neural network in Enshi region, China**

4

5 Bin Zeng^{1,*}, Wei Xiang², Joachim Rohn³, Dominik Ehret⁴, Xiaoxi Chen¹

6

7 1. School of Environmental Studies, China University of Geosciences, Wuhan 430074, Hubei, China

8 2. Faculty of Engineering, China University of Geosciences, Wuhan 430074, Hubei, China

9 3. GeoZentrum Nordbayern, Friedrich-Alexander-Universität Erlangen-Nürnberg, Erlangen 91054, Germany

10 4. Dept. 95 - State Engineering Geology, State Office for Geology, Resources, and Mining, 79104 Freiburg i. Br.,

11 Germany

12

13 * *Corresponding author:* Bin Zeng, Ph.D.

14 Affiliation: School of Environmental Studies, China University of Geosciences.

15 Affiliation address: No. 388 Lumo Road, Wuhan, Hubei, 430074, P.R. China.

16 Email: zengbin_19@126.com. Tel: 86-27-67883473. Fax: 86-27-87436235.



17 **ABSTRACT**

18 Landslides are one of the most common and damaging natural hazards in mountainous areas.
19 However, due to the complex mechanisms that influence the activation of landslides, it can often be
20 very difficult to predict exactly when a landslide will occur. Therefore, research on landslide
21 prevention and mitigation mainly focuses on the distribution forecasting of unstable slopes that are
22 prone to landslides in specific regions and under multiple external forces. The prediction of the spatial
23 distribution of these unstable slopes, termed Landslide Susceptibility Zonation, is important in helping
24 with government land-use planning and in reducing unnecessary loss of life and property. Researching
25 unstable slopes in the Silurian stratum in Enshi region, China, this investigation established a GIS and
26 artificial neural network (ANN)-based method to predict the distribution of potential landslides in this
27 area. Based on the failure mechanism analysis of typical landslides in Silurian stratum, development
28 of evaluation index system which represents the most relevant factors that influence the slope stability,
29 and establishment of intelligent slope stability susceptibility prediction model by artificial neural
30 network, the spatial distribution of unstable slope zones that are prone to landslides were predicted in
31 the study area. The results were further well supported from remote sensing data and field
32 investigations. This research proves that the spatial unstable slope prediction method based on
33 intelligence theory and GIS technology is accurate and reliable.



34 **1 Introduction**

35 Slope failure is a complex natural hazard problem which causes damage to property and loss of life
36 in almost every country. To remedy this, it is necessary to scientifically assess areas that are susceptible
37 to landslide, and so substantially to decrease the damage caused by landslides (Lee et al., 2004). Due to
38 the variety of influencing factors and nonlinear physical processes involved in landslides, it is difficult
39 to predict the potential instability of slope regions where a landslide has not yet occurred.

40 In order to assess the potential for landslide, it is a requirement to identify and analyze the
41 influencing factors first (Lee and Evangelista, 2006). Depending on different landslide types and failure
42 mechanisms, the number of influencing factors was normally decided in the range of 4 to 15 (Shan et al.,
43 2002; Sezer et al., 2011; Pourghasemi et al., 2012; Akgun et al., 2012; Kayasha et al., 2013). Moreover,
44 some researchers analyzed the necessity and weight of different influencing factors (Pradhan and Lee,
45 2010; Ozdermir and Altural, 2013; Mahalinggam et al., 2016), and some researchers analyzed the best
46 forecasting accuracy due to combination of different number of influencing factors (Pradhan and Lee,
47 2010).

48 Afterwards an appropriate and targeted prediction model is the key to the success of landslide
49 susceptibility assessment. To date, a number of different methods combined with GIS have been



50 developed to assess slope stability susceptibility: frequency ratio model and weighting factor method
51 (Yalcin et al, 2011), analytical hierarchy process method (Wang and Yi, 2009), statistical analysis
52 method (Lee and Min, 2001), logistics regression method (Dai and Lee, 2002; Devkota et al., 2012),
53 multi-criteria decision method and likelihood ratio method (Akgun, 2012), evidential belief function
54 model (Althuwaynee et al., 2012), spatial multi-criteria evaluation model (Pourfhasemi et al., 2014),
55 fuzzy overlay method (Kirschbaum et al., 2016), heuristic approach (Ruff and Czurda, 2008), grey
56 clustering method (Zhang et al., 2009), neuro-fuzzy model (Sezer et al., 2011; Bui et al., 2012), and
57 artificial neural network method (Wang et al., 2005; Ercanoglu, 2005; Ermini et al., 2005; Gómez and
58 Kavzoglu, 2005; Lee et al., 2006; Pavel et al., 2007; Wang et al., 2016). Some researchers also
59 compared the predictive capability of different models in the same area and provided recommendations
60 of a more appropriate model (Kanungo et al., 2006; Yalcin et al, 2011; Akgun, 2012; Ozdermir and
61 Altural, 2013; Althuwaynee et al., 2014; pourfhasemi et al., 2014; Goetz et al., 2015; Wang et al., 2016).
62 However, no general agreement has yet been reached about the best method for landslide susceptibility
63 assessment, all known methods have their advantages and disadvantages (Ercanoglu, 2005); but
64 utilization of intelligent method has become more commonly used in recent years.

65 The key problem with the spatial predictions of landslide risk is the establishment of a prediction
66 model that is consistent with the failure mechanism of landslides (Yin, 1992), while the forecast



67 method and criteria are at the core of a forecast model. A large amount of research has been conducted
68 in regards to the spatial prediction of landslides, but there are still some points that can be improved.
69 First, some of the results from the landslide prediction model include the distributions of landslides
70 that have already occurred. However, in these areas the stress accumulated in the slope may have been
71 released through the sliding deformation of the slope, reducing the entire potential energy of the slope
72 to such an extent that these areas are temporarily stable. The real danger lies in slopes that have not
73 yet slid because these could develop into potentially unstable slopes, or even landslides, triggered by
74 various external forces. Therefore, the focus of research to predict the spatial distribution of landslides
75 lies on studying these types of potentially unstable slopes. Secondly, the slope itself is a complex
76 nonlinear, anisotropic body and the external forces are in a non-steady state that is constantly changing
77 in space. Thus, because of the different failure mechanisms of landslides, a targeted mathematical
78 model with the reasonable combination of valuation index system is required for more accurate
79 predictions. Lastly, the prediction of a landslide should include qualitative, quantitative, and
80 experiential factors. Expert knowledge and experience plays a very important role in these
81 predictions, so the combination of expert knowledge and technology will be central to future research
82 on the spatial predictions of landslides.

83 This paper focuses on the distribution of unstable slope zones in the Silurian stratum in Enshi



84 region, China. Based on the failure mechanism analysis of landslides in this specific area, a targeted
85 evaluation factor index system was developed, and a prediction model combined GIS technology with
86 artificial neural network was established for predicting distribution of unstable slope zones that are
87 prone to landslides in the study area. Compare with existing studies, some different attempts have been
88 carried out: (1) the research focused on the distribution of unstable slope zones rather than the existing
89 landslides, since the unstable slopes are more dangerous; (2) this research predicted the unstable slope
90 distribution only in Silurian stratum so as to avoid the interference due to differences in slope failure
91 mechanisms; (3) a “slope structure thematic map” was taken into account to better represent the especial
92 slope failure mechanism in Silurian stratum; (4) replaced the temporal variable of rainfall into a static,
93 spatial variable termed “catchment area” to better act as an influencing factor during the landslide
94 susceptibility. The research results can provide useful guidance for both landslide susceptibility
95 assessment and land planning processes.

96 **2 Background**

97 ***2.1 Geological setting***

98 Enshi is located in the mountainous, southwestern area of the Hubei Province in China, and the
99 study area is located west-north of Enshi region, as shown in Fig.1.

100 For this study, only Silurian stratum (as shown in Fig.2) is chosen as the object stratum in the



101 research area. The benefits of this are clear: in the same stratum, the natural environment, geology and
102 hydrogeology condition, and particularly the failure mechanism, are all convergent, so that the
103 interference due to differences in slope failure mechanisms can be effectively avoided.

104 The study area is located in a mountainous area that ranged in elevation from 600 to 1200 m. The
105 surface water system is well developed; the rivers are generally between 20 and 40 m wide. There are
106 slopes on both sides of the valley and gully, generally with slope angles of 20°-40°. The valley is
107 V-shaped with a relative elevation from the bottom to the ridge between 200 and 600 m. Large ancient
108 debris deposits are distributed along the river and its tributaries.

109 The components of the Silurian stratum are mainly shale, mudstone, siltstone, silty mudstone,
110 silty clay, pelitic siltstone and other clastic rocks. The lithological strength is weak. Various external
111 geological effects, such as unloading, rainfall infiltration and erosion, and wind weathering, could
112 easily destroy the rock mass structure and provide a wealth of material for landslides. The main
113 components of loose soil are clay and silt clay with fragments. The main causes of formation are
114 eluvium, alluvium and colluvium. Generally, the thickness of loose soil is 0.5-10 m, with a maximum
115 thickness of 15 m. Due to the loose structure, and low physical and mechanical strength, the surface
116 loose soil can be easily turned into shallow landslide.

117 ***2.2 Mechanism analysis of shallow landslides in the Silurian stratum***



118 2.2.1 Characteristics of landslides in the Silurian stratum

119 According to the filed investigation and statistic results, most of the landslides in Silurian stratum
120 in the study area are soil landslides (81.3%), with a volume of less than 10^6 m^3 (81%), a slope angle
121 between 15° and 35° (82%), a thickness of less than 10 m (75%) or between 10 and 25 m (16%), and
122 they occurred during the rainy season from June to August (87.5%).

123 2.2.2 Geological and environmental conditions for the shallow landslides

124 The conditions causing shallow soil landslides (some examples in Fig.3) in the Silurian stratum are
125 related to the following factors. First, most of the slopes were between 10 and 200 m high and had free
126 surface in front. Second, most of the landslide bodies were weathered and loosely accumulated, with a
127 thickness of 2 to 10 m. Third, dip slope or skew slope (slope with a small angle between slope surface
128 dip direction and stratum dip direction, as defined in Table 1) structure provided conditions of slide
129 surface. Fourth, the upper loose soil layer had weak permeability and strong water-holding capacity,
130 while the underlying bedrock was a relative aquifuge. Thus, the upper soil layer was easily soaked and
131 softened to form a slide surface near the interface of the soil layer and bedrock. Fifth, because the
132 mechanical strength of the soil was low, when the water content was increased, the shear strength (τ)
133 decreased rapidly. Finally, long-term, heavy rainfall, and slope cutting were the main external factors
134 that triggered shallow soil landslides in the study area.



135 2.2.3 Evolution of shallow landslides in the Silurian stratum

136 Based on the analysis of the factors influencing the slope stability, a typical failure mechanism of
137 shallow landslides in Silurian stratum is described here. This process occurs after the accumulation
138 body has been formed on the bedrock. Often during rain events, a tension crack in the trailing edge of
139 the accumulation body appears at the top, extending to both sides. The tension fracture becomes a
140 major channel for surface water infiltration. In continuous rainfall conditions, there is also continuous
141 runoff of surface water and infiltration along the fracture channel. Water erosion washes out and
142 further loosens the soil along the fracture, which widens and deepens the cracks, extending the trailing
143 edge of the tension crack and gradually forming the sliding surface. However, due to the clay gravel
144 composition of the accumulation body, the infiltration of groundwater discharge is blocked. This
145 increase pore water pressure and decreases the effective stress of the accumulation body, especially
146 near the trailing edge of the cracks, which reduces the friction force between the particles. At the same
147 time, because the weight of the slope body has increased, the shear stress in the front edge of the
148 accumulation body gradually increases to a maximum intensity. The shear strength is gradually
149 reduced and the middle part of the slope body (locking section) reaches its peak strength. With further
150 deformation of the accumulation body, the strength of the soil mass is reduced, the sliding surface
151 joins, and the total anti-sliding force (shear strength) of the sliding surface nearly equals the total



152 sliding force until the landslide occurs.

153 **3 Methods**

154 ***3.1 Establishment of an influencing factor system of the shallow landslide***

155 3.1.1 Screening of the index factors

156 Although there are several geological, topographical, and/or environmental parameters that can be
157 used to produce landslide susceptibility thematic maps, selection of these parameters depends on several
158 factors such as data availability, data quality, size of the study area, scale of the work, user experience
159 etc (Ercanoglu, 2005). For this study, according to the failure mechanism analysis of the shallow
160 landslides in Silurian stratum, except lithology factor, four most relevant landslide influence factors
161 (slope angle, slope structure, road influence and rainfall) were identified:

162 (1) Slope angle

163 The slope angle determines the distribution of the landslide based on the geometric features, and
164 also directly determines the stress distribution in the slope. Different slope angles not only affects the
165 magnitude of the residual stress along the existing or potential sliding surfaces but also determines the
166 form and mechanism of slope deformation failure. Controlled by topography, landslides in Silurian
167 stratum generally occurred in slopes with angles of 15°-35°, which accounted for approximately 82%
168 of all landslides in the same stratum.



169 (2) Slope structure

170 According to the field survey, most of the shallow landslides in Silurian stratum have occurred
171 either in dip slopes or in skew slopes (slope with a small angle between the slope surface dip direction
172 and stratum dip direction, as defined in Table 1). Because the sliding surface normally locates near the
173 separation plane of the loose soil layer and bedrock, when the slope aspect and dip direction of the
174 stratum are the same or intersect in a small angle, the sliding surface effect reflects more clearly.

175 (3) Road influence

176 The landslides in Enshi region are clearly influenced by human activities. The total number of
177 landslides and unstable slopes caused by human activities was 83% and mainly included slope cutting
178 during the construction of roads.

179 (4) Rainfall

180 Rainfall was the most active element that caused landslides in Silurian stratum. First, rainfall was
181 converted partly into surface runoff. Then, after the runoff continued for a long time, it formed a gully
182 on the surface that changed the surface morphology of the slope. After the gully was eroded deep
183 enough, it would provide the spatial conditions necessary for the deformation and failure of the slope.
184 In Enshi region according to field investigations, most of the landslide toes were distributed in stream
185 systems or gullies and the slope toe was constantly eroded which provided a free surface for the final



186 destruction of the slope.

187 Rainfall is a temporal variable, but for a spatial distribution prediction of landslides it should have
188 the characteristics of a spatial variable. Due to the importance of rainfall as an influencing factor, it is
189 necessary to change this factor from a temporal variable to a static evaluation index with spatial
190 distribution characteristic. Therefore, the concept of a “catchment area” is established. This represents
191 the capacity of slopes to collect surface water that has been transformed from rain. As shown in Fig.4,
192 using the catchment area concept, the temporal variable of rainfall is converted into a static spatial
193 variable and related to the slope stability.

194 3.1.2 Quantification of indices

195 The evaluation index is divided into qualitative and quantitative indices, which must be given a
196 quantitative value. In addition, the variables must all undergo compression processing or
197 non-dimensional data processing before they are used (Wang, 2000). Because the measurement units
198 of each variable are inconsistent, different variables have different levels of influence and some are
199 exaggerated, so it is necessary to eliminate the dimensional effect of the variables. In this study,
200 continuous variable indices, linear factor indices, and discrete variable indices are distinguished.

201 (1) Continuous variable index: slope angle

202 According to the difference principle, the relationship between landslide distribution density and



203 the slope angle in the study area are combined, and the slope angle is divided into four ranges, 0°-15°,
204 15°-35°, 35°-50°, 50°-90°, so as to make the division of continuous variable states more reasonable,
205 and the prediction model more optimized.

206 (2) Linear factor indices: road influence buffer zone, stream system and gully influence buffer
207 zone

208 To deal with linear factors, it is necessary to determine the distance between landslides and these
209 types of factors, using the buffer analysis principle and statistical analysis to determine the radius of
210 influence. In addition, the minimum grid size for the spatial analysis, considered to be 50 m for
211 statistical analyses, is used. Considering the frequency of landslide distributions at different buffer
212 distances, the SC (Susceptibility Coefficient) method shown in Eq. (1) is adopted to obtain a
213 reasonable buffer distance.

$$214 \quad SC_i = \ln \left(\frac{N_i}{A_i} / \frac{N}{A} \right) \quad (1)$$

215 SC_i – the sensitivity coefficient of a certain type in factor i (greater value indicates that a landslide
216 will occur easier in this section); N_i – the number of landslides of a certain factor, i (type); A_i – the
217 area (km^2) of a certain factor i ; N – the total number of landslides in the study area; A – the total study
218 area (km^2).

219 According to this, the SC values representing the influence of the distance from stream systems



220 and roads can be calculated. The influence radius of the stream systems and gullies is 50 m and the
221 influence radius of the road is 100 m.

222 (3) Discrete variable index: slope structure

223 Based on the angle between the slope surface dip direction and stratum dip direction, the slope
224 structure can be divided into three main types: dip slope, reverse slope, and skew slope (Hoek & Bray,
225 1981). Based on the field investigation experience about slope stability, the slope stability from best
226 to worst is: reverse slope > skew slope > dip slope.

227 In the process of extraction, the stratum dip directions are divided into 8 ranges: 0°-45°, 45°-90°,
228 90°-135°, 135°-180°, 180°-225°, 225°-270°, 270°-315°, 315°-360°. Based on the stratum dip direction
229 and slope surface dip direction distribution maps calculated by ArcGIS, the angle between the slope
230 surface dip direction and the stratum dip direction is obtained by subtracting the superposition
231 calculation from the above two layers. The slope structure is divided into regions in the study area
232 according to Table 1.

233 3.1.3 Weight of index

234 The intelligent prediction system used in this paper is based on the neural network learning
235 memory sample rule that simulates the thinking in a human brain and automatically assigns weight
236 coefficients during the process of forecast calculations. The advantage of this computing process is



237 that it can effectively avoid the interference of human factors. However, the prediction system is based
238 on the thinking method of the human brain; therefore, the neural network method requires high
239 quantities of typical samples for correct learning and forecasting.

240 ***3.2 Establishment of an artificial neural network prediction model***

241 3.2.1 Selection and prediction process of a neural network model

242 A BP (Back Propagation) neural network is a type of neural network that has a one-way
243 transmission of multilayer, feed-forward neural networks. A neuron is the basic unit of the neural
244 network. In the network, the neurons are arranged in layers that are composed of the input layer, the
245 hidden layer (of which there can be several) and the output layer. Because the prediction of unstable
246 slopes in theory is a process of functional approximations, then based on the influence factor
247 parameters in the input layer, the nonlinear mapping relationship with the corresponding output
248 parameters can be obtained (Zhang et al., 2005). Therefore, a BP neural network is very suitable for
249 addressing the prediction of unstable slopes.

250 The steps (flow-chart as shown in Fig.5) involved in using a BP neural network to predict the
251 distribution of unstable slope zones is as follows: First, typical and investigated unstable slopes are
252 used as the research objects. Various factors that may affect the stability of the slope are quantified to
253 be the input values of the input layer nodes. The stability state of these slopes is divided, quantified,



254 and regarded as the desired output of the output layer nodes. Then, the neural network is repeatedly
255 trained using these known samples until the total error of the network meets the precision requirement.
256 In this way, the network masters the relationship between the input factors and the expected output.
257 Finally, the input includes the influence factors of slope stability for unknown regions, and based on
258 the previously established and tested neural network prediction model, the spatial unstable slopes
259 distribution result for unknown region can directly obtained.

260 3.2.2 Construction of a BP neural network model

261 Determine the number of neurons for the input and output layers. Based on the previous
262 analysis of slope stability influence factors, the number of neurons in the input layer is 4 and the
263 number of neurons in the output layer is 1, which is the stability state of the slope.

264 Determine the number of hidden layers in the neural network. Any continuous function on a
265 closed interval can be approached by single hidden layer BP network. Thus, a three BP network can
266 complete any of n-dimensional to m-dimensional mappings (Feng et al., 2009). Therefore, the hidden
267 layer of this BP network is set to 1.

268 Determine the number of neurons in the hidden layer. According to the Kolmogrov theorem (Wen,
269 2004), given any continuous function $f: [0,1]^n \rightarrow R^m$, f can be achieved through a three layer
270 forward neural network. The input layer has n neurons, the middle layer has $2n + 1$ neurons, and the



271 output layer has m neurons. Therefore, the neuron number of the hidden layer is: $2 \times 4 + 1 = 9$.

272 Determine the network training function. The “traingdx” function (momentum and adaptive
273 algorithm) can not only effectively avoids the problem of local minima but also adjusts the learning
274 rate. Therefore, it has high training efficiency and a stable training process (Wen, 2004), and is chosen
275 as the training function for the neural network.

276 Determine the initial weights and threshold values for the neural network. Based on a comparison
277 of different initial ranges, it is found that an initial value which is not too large has little impact on the
278 overall performance of the network, while a smaller initial range is more conducive to uniformly
279 random initial weights (Freeman, 1993). In the BP neural network, the initial network weights and
280 thresholds are given random values in the acceptable range. Finally, the structure of the designed BP
281 network is shown in Fig.6:

282 3.2.3 Pretreatment of sample data

283 The prediction principle of neural networks is that the neural network can effectively approximate
284 the inherent laws of the sample by studying and remembering the known samples, then carry out an
285 associated forecast according to the memory. Thus, the unknown samples to be predicted must be
286 similar to the known samples. At the same time, the known samples should also cover as much as
287 possible the different combinations of various factors to improve the forecasting ability of the network



288 (Zhang, 2006).

289 Sample data: 35 stable and unstable slopes in Silurian stratum in Enshi region are chosen as the
290 sample data, as shown in Fig.7. The recognition and mapping have been carried out by
291 geomorphological field survey. The defined unstable slopes are slopes that have deformation evidence,
292 and may prone to typical shallow soil landslides in Silurian stratum under multiple external forces. As
293 shown in Table 2, samples 1-25 are used for the network training and samples 26-35 are used to test
294 the performance of the network prediction.

295 Reprocessing of sample data: The response of neurons is between 0 (inhibition) and 1 (activation).
296 To ensure that the BP neural network learns as best as possible and to prevent small numerical
297 variables in the input from being overwhelmed by large numerical data, the sample data are
298 normalized before processing. Input values are converted to values between 0-1 with an appropriate
299 transformation. For the qualitative index, the ones and zeros of the binary logic calculations can be
300 used to express yes or no for the categories; for other indexes, the values were corresponding to
301 between 0.1 and 0.9 according to their contribution. As shown in Table 2.

302 3.2.4 Training and testing the forecasting ability of the established neural network model

303 (1) Training procedure

304 Based on MATLAB 7.1, the established neural network model was trained using samples 1-25:



305 The training code in MATLAB is as follow:

306 netgdx=newff (minmax (p1) , [9, 1], {'tansig', 'logsig'}, 'traingdx', 'learnqdm', 'mse') ;

307 netgdx.trainParam.epochs=10000;

308 netgdx.trainParam.goal=0.00001;

309 netgdx =train (netgdx, p1, t1) ;

310 The training result is shown in Fig.8:

311 (2) Testing procedure

312 After the neural network had been trained and achieved the training goal, samples 26-35 were
313 used to test the predictive ability of the network. As shown in Table 3, the prediction accuracy for
314 samples 26-35 reached 80%. Therefore, the network was considered to have reached a stable state
315 with a good forecasting ability.

316 **4 Results and Discussion**

317 ***4.1 Implementation of the spatial prediction for unstable slopes in the study area***

318 According to the analysis of main influencing factors based on slope failure mechanism in the
319 research area, four evaluation indices were taken into account during the prediction model, including:
320 slope angle, slope structure, influence buffer of streams and gullies, and influence buffer of roads.

321 Classification of the forecast unit in the study area: The spatial database of the thematic layer is



322 often vector data. When predicting the landslide susceptibility, it is necessary to convert the vector
323 data into raster data, which is the grid processing by ArcGIS. Based on topographical and geological
324 maps, the four thematic layers were gridded using 25 m x 25 m by ArcGIS. After gridding, the total
325 raster number in the study area was 81382, and in the actual calculations in Silurian stratum the total
326 area was approximately 103 km².

327 Creation of the impact factor thematic layer: the four parameters, which were used in the landslide
328 susceptibility in this study, were derived from remote sensing data, DEM and ancillary data from
329 fieldwork. The distribution of slope angle thematic map was calculated by the digital terrain analysis
330 function in ArcGIS; the distribution of road influence buffer and distribution of stream and gully
331 influence buffer thematic maps were calculated by the buffer analysis function in ArcGIS; for the
332 distribution of slope structure thematic map, firstly the distribution of slope aspect thematic map was
333 calculated by ArcGIS based on DEM data, then the distribution of bedrock dip direction thematic map
334 was gained according to geologic map and field investigation, finally the distribution of slope
335 structure thematic map can be obtained by overlying the above two thematic maps in ArcGIS. The
336 four thematic layers were obtained as shown in Fig.9.

337 ***4.2 Distribution of unstable slope zones in the Silurian Stratum***

338 Based on a GIS superposition calculation of the four thematic layers, the predicted result of the



339 spatial distribution of unstable slopes in the study area was obtained, as shown in Fig.10.

340 As shown in Fig.10, the red areas are natural slopes which have not completely slid, but under the
341 continuing influence of external forces (i.e., rainfall, earthquakes, large-scale human engineering
342 activities, etc.) these areas will likely form shallow soil landslides in the Silurian stratum. In addition,
343 the potential instability region (red) in Fig.10 does not fully represent the exact boundaries of a single
344 slope that may slide in the future. If the slopes become unstable in the future, these regions will be the
345 origins of slope failure. Therefore, understanding the distribution of these regions is of great
346 importance for further determinations of the approximate ranges of unstable slopes.

347 The results also showed that the Neural Network Intelligent Forecasting System based on
348 repetitive learning and memory of a representative sample, under the premise of mastering the special
349 regularity of the Silurian stratum slope failure, was sufficient to dynamically assess weights for the
350 various factors. Although the weight of each impact factor is different, a landslide cannot be triggered
351 only by a single factor. Multiple factors in different combinations were given different weights by the
352 intelligence system, which not only improved the accuracy of predictions of regional slope stability
353 under complex topographic and geologic conditions but also avoided the errors associated with
354 subjective decisions about the weight of each factor.

355 ***4.3 Accuracy verification of the spatial prediction model***



356 To further verify the accuracy of the intelligent prediction model, the predicted potentially
357 unstable region was verified by both remote sensing data (SPOT-5 satellite with resolution of 2.5 m)
358 and field investigations, as shown in Table 4.

359 The unstable slope zones determined by the result of the intelligent prediction are closely
360 reflected in the data determined from remote sensing and confirmations made through field
361 investigation. This proves that the intelligent prediction of unstable slopes based on a neural network
362 results in an accurate forecast, especially for shallow soil slope failure zones in Silurian stratum.

363 The good judgment exhibited by the intelligent forecasting system in regards to the influence of
364 slope gullies greatly improves the accuracy of the prediction. It is found from the predicted results that
365 most of the unstable slope zones, either at the toe or on sides of the border, are distributing along
366 continuous gullies that provide a free surface for slope deformation and failure. This is consistent with
367 the failure mechanism of landslides in Silurian stratum. It also highlights the benefit of stream and
368 gully distribution maps based on the catchment area concept. Compared with the traditional single
369 stream distribution map, the model is able to judge the distribution of the gullies in non-perennial
370 water areas, and these gullies have played a very important role in the occurrence of Silurian stratum
371 landslides.



372 As for results of the intelligent spatial prediction of unstable slopes, it cannot completely
373 represent the precise scope of each potentially unstable slope body and what is more significant is the
374 information about the initial damage site of unstable slope body. Therefore, in actual use, the predicted
375 potential instability region should also be combined with field surveys to determine the accurate range
376 of unstable slopes which would be destroyed by external forces in the future.

377 **5 Conclusions**

378 This paper established a relatively complete method for the spatial prediction of unstable slope
379 zones in the Silurian stratum in Enshi region that used slope failure mechanism analysis, GIS-based
380 data collection, evaluation index system development, ANN-based intelligent unstable slope
381 prediction model design. According to the results of remote sensing data and field investigation, the
382 prediction model is accurate and reliable. This method will be useful for the prediction of similar slope
383 disasters in mountainous area.

384 The study also made the following different attempts compare with other researches: (1) selected
385 a single Silurian stratum as study object to effectively avoid errors in forecast accuracy due to
386 different slope failure mechanisms in different strata; (2) focused on the prediction of spatial
387 distribution of unstable slopes rather than existing landslides, since unstable slopes are much more
388 dangerous; (3) established the concept of “catchment area”, so that rainfall can be indirectly



389 considered as a static, spatial evaluation index associated with slope stability, the use of “catchment
390 area” is also able to accurately describe the gully distribution which plays a crucial role in slope
391 stability; (4) established a slope structure thematic map which well reflects the specific failure
392 mechanism of shallow soil landslides in Silurian stratum.

393 **Author Contributions**

394 Bin Zeng contributed to data analysis and manuscript writing; Wei Xiang, Joachim Rohn and
395 Dominik Ehret proposed the main structure and key idea of this study; Xiaoxi Chen performed the
396 ANN calculation. All authors read and approved the final manuscript.

397 **Acknowledgments**

398 This work was supported by the open fund from Three Gorges Research Center for geo-hazards,
399 Ministry of Education, China [grant numbers: TGRC201007]; the national study abroad fund for
400 construction of high level university, China [grant number: 20073020].

401 **Conflicts of Interest**

402 The authors declare that they have no conflict of interest.



403 **Reference**

- 404 Akgun, A., Sezer, E.A., Nefeslioglu, H.A., Gokceoglu, C. and Pradhan, B.: An easy-to-use MATLAB
405 program (MamLand) for the assessment of landslide susceptibility using a Mamdani fuzzy
406 algorithm. COMPUT GEOSCI-UK, 38, 23-34, 2012.
- 407 Akgun, A.: A comparison of landslide susceptibility map sproduced by logistic regression,
408 multi-criteria decision, and likelihood ratio methods: a case study at zmir, Turkey. Landslides, 9,
409 93-106, 2012.
- 410 Althuwaynee, O.F., Pradhan, B. and Lee, S.: Application of an evidential belief function model in
411 landslide susceptibility mapping. COMPUT GEOSCI-UK, 44, 120-135, 2012.
- 412 Althuwaynee, O.F., Pradhan, B., Park, H.J. and Lee, J.H.: A novel ensemble bivariate statistical
413 evidential belief function with knowledge-based analytical hierarchy process and multivariate
414 statistical logistic regression for landslide susceptibility mapping. Catena, 114, 21-36, 2014.
- 415 Bui, D.T., Pradhan, B., Lofman, O., Revhaug, I. and Dick, O.B.: Landslide susceptibility mapping at Hoa Binh
416 province (Vietnam) using an adaptive neuro-fuzzy inference system and GIS. COMPUT
417 GEOSCI-UK, 45, 199-211, 2012.
- 418 Dai, F.C. and Lee, D.F.: Landslide characteristics and slope instability modeling using GIS, Lantau



-
- 419 Island, Hong Kong. *Geomorphology*, 48, 213-228, 2002.
- 420 Devkota, K.C., Regmi, A.D., Pourghasemi, H.R., Yoshida, K., Pradhan, B., Ryu, I.C., Dhital, M.R. and
421 Althuwaynee, O.F.: Landslide susceptibility mapping using certainty factor, index of entropy and
422 logistic regression models in GIS and their comparison at Mugling–Narayanghat road section in
423 Nepal Himalaya. *Nat Hazards*, 65, 135-165, 2012.
- 424 Ercanoglu, M.: Landslide susceptibility assessment of SE Bartın (West Black Sea region, Turkey) by
425 artificial neural networks. *NAT HAZARD EARTH SYS*, 5, 979-992, 2005.
- 426 Ermini, L., Catani, F. and Casagli, N.: Artificial Neural Networks applied to landslide susceptibility
427 assessment. *Geomorphology*, 66, 327-343, 2005.
- 428 Freeman, J.A.: *Simulating Neural Networks with Mathematica*. Addison-Wesley, Reading, Ma, 1993.
- 429 Feng, H.Z., Li, W. and Ma, T.H.: Geological disasters early warning and forecast
430 information-releasing system: a new generation of releasing system based on ANN and GIS.
431 *Journal of natural disasters*, 18, 187-193, 2009.
- 432 Gómez, H., Kavzoglu, T.: Assessment of shallow landslide susceptibility using artificial neural
433 networks in Jabonosa River Basin, Venezuela. *ENG GEOL*, 78, 11-27, 2005.
- 434 Goetz, J.N., Brenning, A., Petschko, H. and Leopold, P.: Evaluating machine learning and statistical
435 prediction techniques for landslide susceptibility modeling. *COMPUT GEOSCI-UK*, 81, 1-11,



-
- 436 2015.
- 437 Hoek, E. and Bray, J.W.: Rock Slope Engineering, third ed. E & FN SPON, New York, 1981.
- 438 Kanungo, D.P., Arora, M.K., Sarkar, S. and Gupta, R.P.: A comparative study of conventional, ANN
439 black box, fuzzy and combined neural and fuzzy weighting procedures for landslide susceptibility
440 zonation in Darjeeling Himalayas. ENG GEOL, 85, 347-366, 2006.
- 441 Kayastha, p., Dhital, M.R. and Smedt, F.D.: Application of the analytical hierarchy process (AHP) for
442 landslide susceptibility mapping: A case study from the Tinau watershed, west Nepal. COMPUT
443 GEOSCI-UK, 52, 398-408, 2013.
- 444 Kirschbaum, D., Stanley, T. and Yatheendradas, S.: Modeling landslide susceptibility over large
445 regions with fuzzy overlay. landslides, 13, 485-496, 2016.
- 446 Lee, S. and Min, K.: Statistical analysis of landslide susceptibility at Yongin, Korea. ENVIRON
447 GEOL, 40, 1095-1113, 2001.
- 448 Lee, S., Ryu, J.H., Won, J.S. and Park, H.J.: Determination and application of the weight for landslide
449 susceptibility mapping using an artificial neural network. ENG GEOL, 71, 289-302, 2004.
- 450 Lee, S. and Evangelista, D.G.: Earthquake-induced landslide-susceptibility mapping using an artificial
451 network. NAT HAZARD EARTH SYS, 6, 687-695, 2006.
- 452 Lee, S., Ryu, J.H. and Lee, M.J.: The Application of Artificial Neural Networks to Landslide



-
- 453 Susceptibility Mapping at Janghung, Korea. *Mathematical Geology*, 38, 199-220, 2006.
- 454 Mahalingam, R., Olsen, M.J. and O'Banion, M.S.: Evaluation of landslide susceptibility mapping
455 techniques using lidar-derived conditioning factors (Oregon case study). *GEOMAT NAT HAZ*
456 *RISK*, 7, 1884-1907, 2016.
- 457 Ozdermir, A. and Altural, T.: A comparative study of frequency ratio, weights of evidence and logistic
458 regression methods for landslide susceptibility mapping: Sultan Mountains, SW Turkey. *J ASIAN*
459 *EARTH SCI*, 64, 180-197, 2013.
- 460 Pavel, M., Fannin, R.J. and Nelson, J.D.: Replication of a terrain stability mapping using an Artificial
461 Neural Network. *Geomorphology*, 97, 356-373, 2007.
- 462 Pradhan, B., Lee, S.: Landslide susceptibility assessment and factor effect analysis: backpropagation
463 artificial neural networks and their comparison with frequency ratio and bivariate logistic
464 regression modeling. *ENVIRON MODELL SOFTW*, 25, 747-759, 2010.
- 465 Pradhan, B. and Lee, S.: Regional landslide susceptibility analysis using back-propagation neural
466 network model at Cameron Highland, Malaysia. *Landslides*, 7, 13-30, 2010.
- 467 Pourghasemi, H.R., Pradhan, B. and Gokceoglu, C.: Application of fuzzy logic and analytical
468 hierarchy process (AHP) to landslide susceptibility mapping at Haraz watershed, Iran. *Nat*
469 *Hazards*, 63, 965-996, 2012.



-
- 470 Pourghasemi, H.R., Moradi, H.R., Aghda, S.M.F., Gokceoglu, C. and Pradhan, B.: GIS-based
471 landslide susceptibility mapping with probabilistic likelihood ratio and spatial multi-criteria
472 evaluation models (North of Tehran, Iran). Arab J Geosci, 7, 1857-1878, 2014.
- 473 Ruff, M. and Czurda, K.: Landslide susceptibility analysis with a heuristic approach in the Eastern
474 Alps (Vorarlberg, Austria). Geomorphology, 94, 314-324, 2008.
- 475 Shan, J.X., Ye, H. and Li, Z.F.: Prediction method of dangerous areas of regional landslide based on
476 GIS and its application. Chinese Journal of Rock Mechanics and Engineering, 21, 1507-1514,
477 2002.
- 478 Sezer, E.A., Pradhan, B. and Gokceoglu, C.: Manifestation of an adaptive neuro-fuzzy model on
479 landslide susceptibility mapping: Klang valley, Malaysia. EXPERT SYST APPL, 38, 8208-8219,
480 2011.
- 481 Wang, X.C.: Study of some key issues about the 3S forecast system for landslide of the three gorges
482 area. PhD Thesis, Beijing Geotechnique Institute of CUMT, China, 2000.
- 483 Wang, H.B., Xu, W.Y. and Xu, R.C.: Slope stability evaluation using Back Propagation Neural
484 Networks. ENG GEOL, 80, 302-315, 2005.
- 485 Wang, Z. and Yi, F.C.: AHP-based evaluation of occurrence easiness of geological disasters in
486 Mianyang City. Journal of natural disasters, 18, 14-23, 2009.



-
- 487 Wen, H.J.: A study on intelligence system supported by GIS and its application of landslide-forecast.
488 PhD Thesis, Chongqing University, China, 2004.
- 489 Wang,L.J., Guo, M., Sawada, K., Lin, J. and Zhang, J.C.: A comparative study
490 of landslide susceptibility maps using logistic regression, frequency ratio, decision tree, weights
491 of evidence and artificial neural network. GEOSCI J, 20, 117-136, 2016.
- 492 Yin, K.L.: Reviews on the prediction of landslide hazard. Geological sciences and technology
493 information, 11, 59-62, 1992.
- 494 Yalcin, A., Reis, S. and Aydinoglu, A.C.: A GIS-based comparative study of frequency ratio,
495 analytical hierarchy process, bivariate statistics and logistics regression methods for landslide
496 susceptibility mapping in Trabzon, NE Turkey. Catena, 85, 274-287, 2011.
- 497 Zhang, Y.X., Wen, H.J. and Ou, M.: Intelligent prediction theory and its application of landslide.
498 Science Press, Beijing, 2005.
- 499 Zhang, G.R.: Spatial prediction and real-time warning of landslide and it's risk management based on
500 webgis. PhD Thesis, China University of Geosciences, China, 2006.
- 501 Zhang, L., Li, G.J. and Zhou, Z.G.: Grey clustering method-based zoning assessment of regional
502 geological disaster. Journal of natural disasters, 18, 164-168, 2009.



Figure captions

Fig. 1. The location of the study area.

Fig. 2. Generalized geological map. Only Silurian stratum is chosen as the study area.

Fig. 3 Typical shallow soil landslides in the Silurian stratum in Enshi region.

Fig. 4 Conversion of the temporal variable of rainfall into a static, spatial variable termed “catchment area” to better act as an influencing factor during the slope stability susceptibility

Fig. 5 Flow-chart methodology for the prediction of unstable slope distribution in the Silurian stratum in Enshi region based on BP neural network.

Fig. 6 The structure of the BP neural network model for the prediction of unstable slope zones in Silurian stratum

Fig. 7 Stable and unstable slopes inventory map of the study area. The recognition and mapping have been carried out by geomorphological field survey.

Fig. 8 Training procedure and error curve of the neural network model based on “traingdx” training function. During the training process, the error curve had good convergence and met the training goal within setting epochs, which means the “traingdx” training function can make the model has a stable training process and expected training result.

Fig. 9 (a) Distribution of slope angle; (b) Distribution of road influence buffer; (c) Distribution of



stream and gully influence buffer; (d) Distribution of slope structure.

Fig. 10 Results of the slope stability susceptibility assessment performed by the BP neural network in the Silurian stratum in Enshi region.

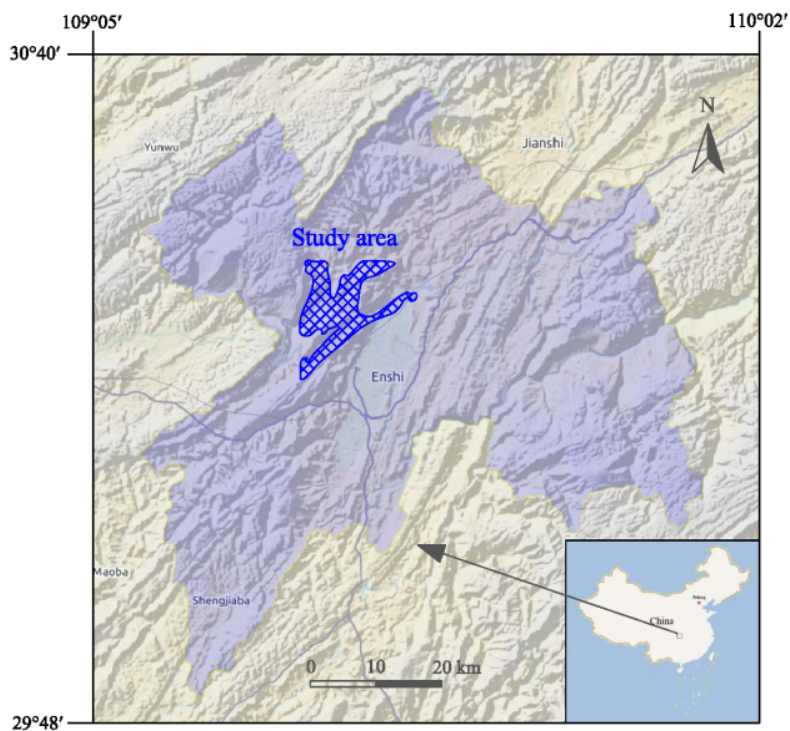


Fig.1

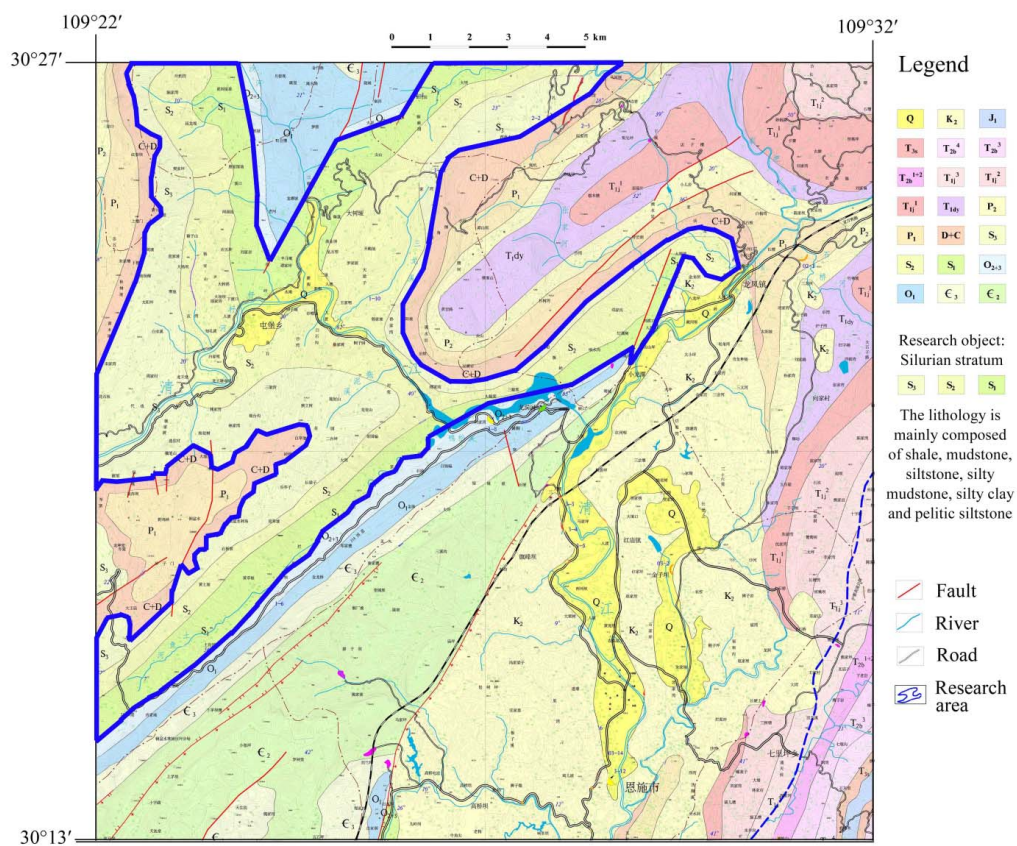


Fig.2

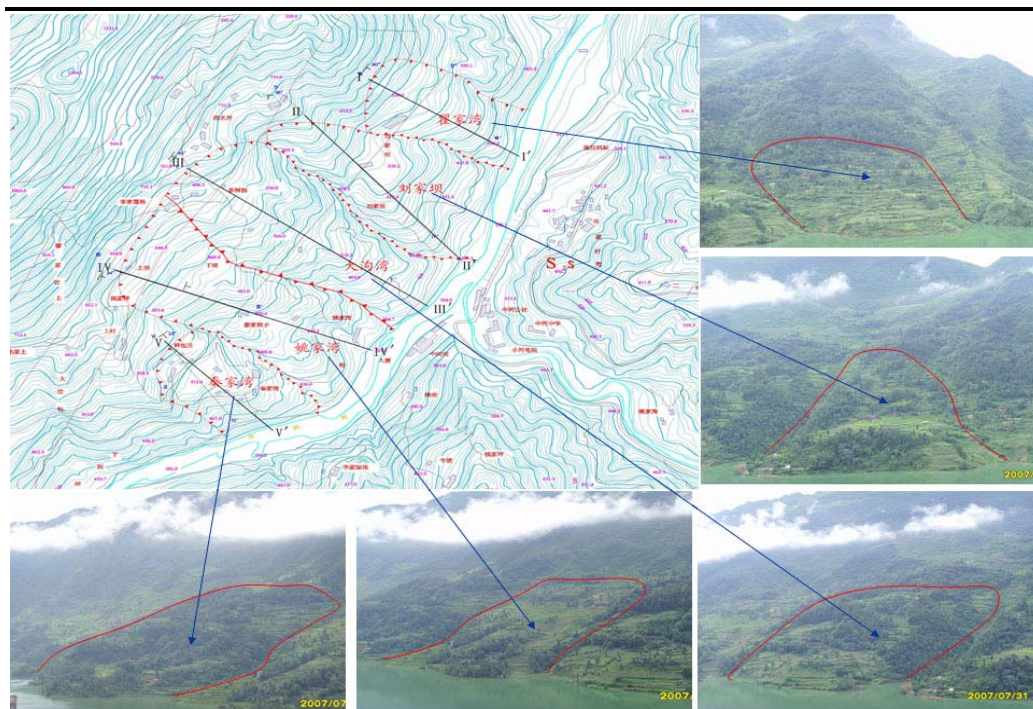


Fig.3

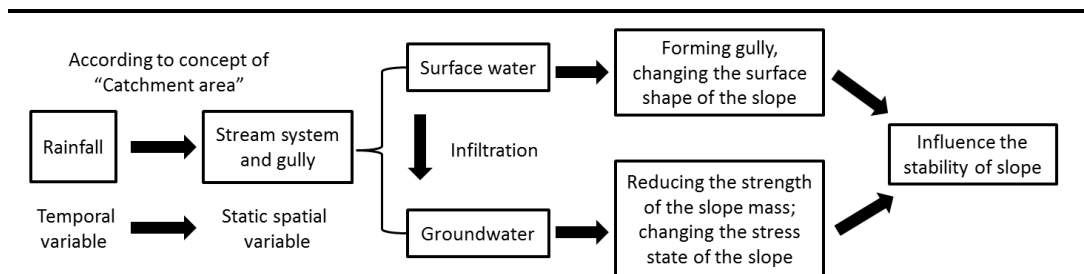


Fig.4

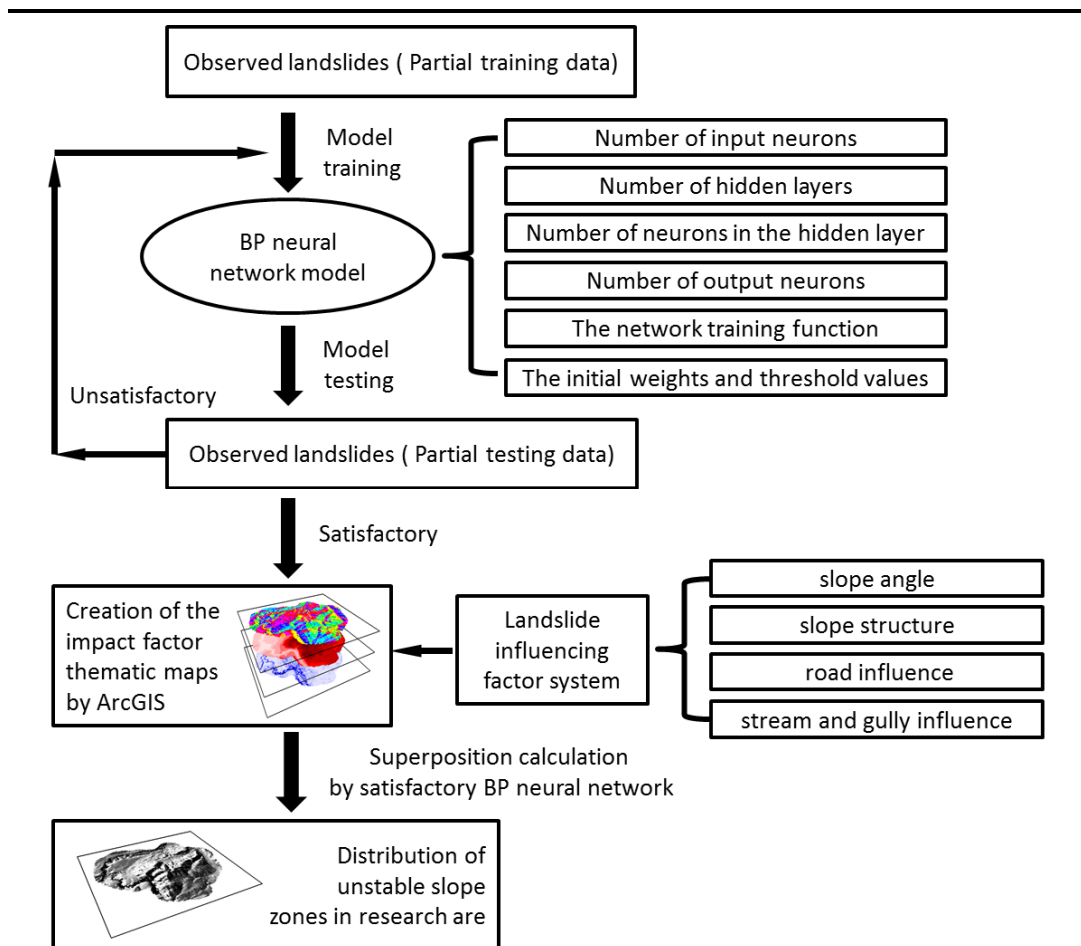


Fig.5

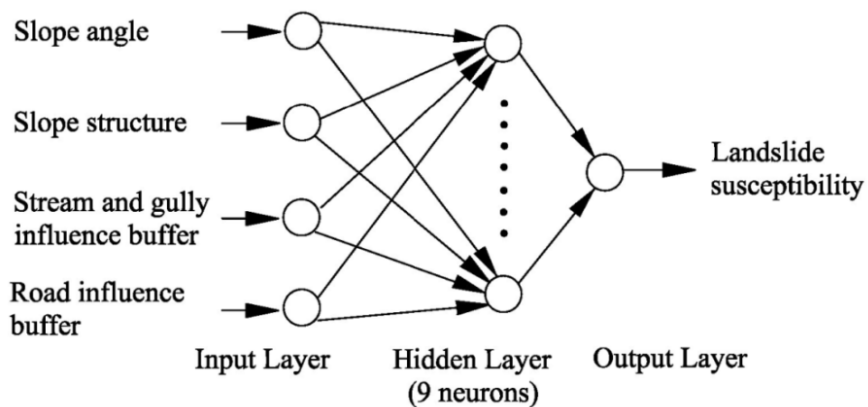


Fig.6

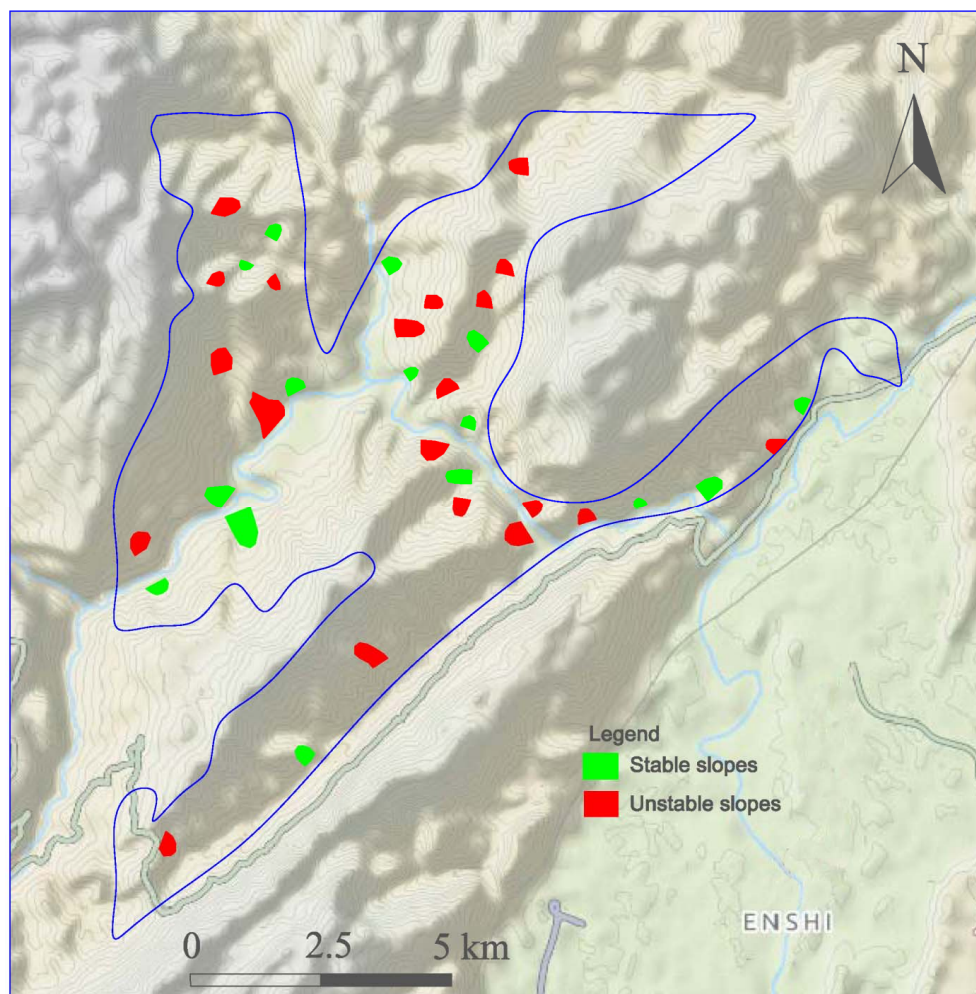


Fig.7

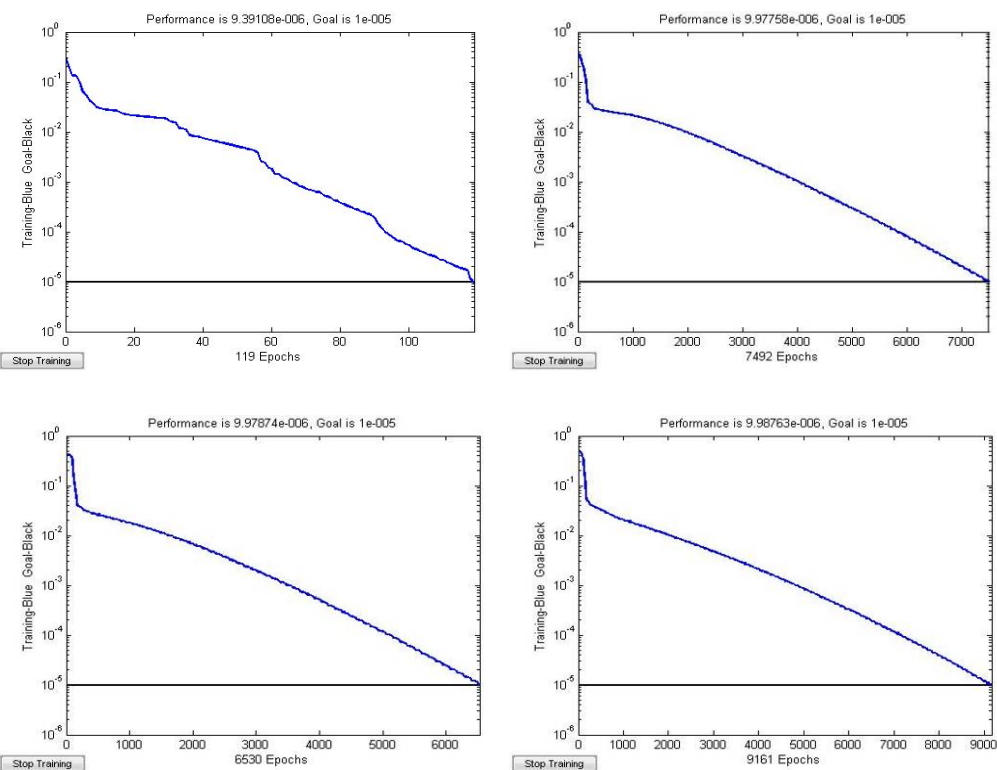


Fig.8

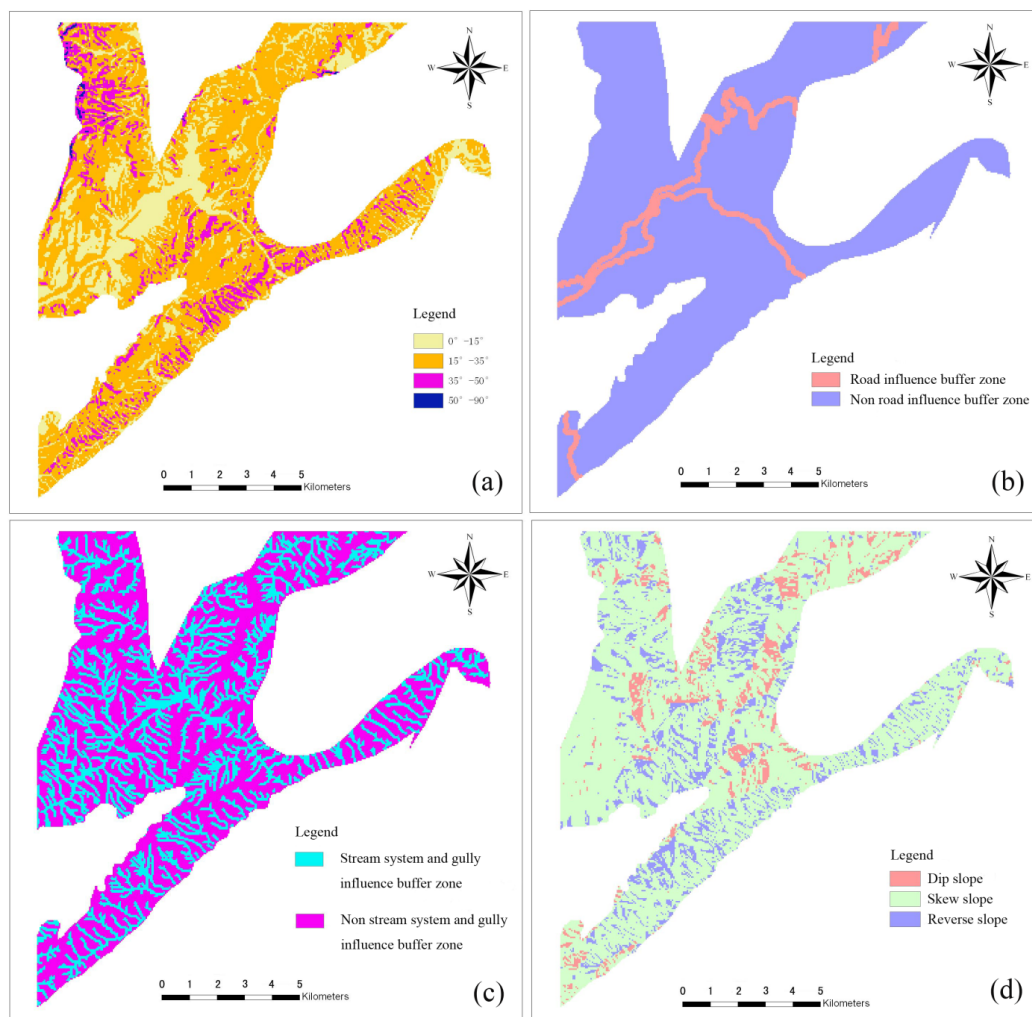


Fig.9

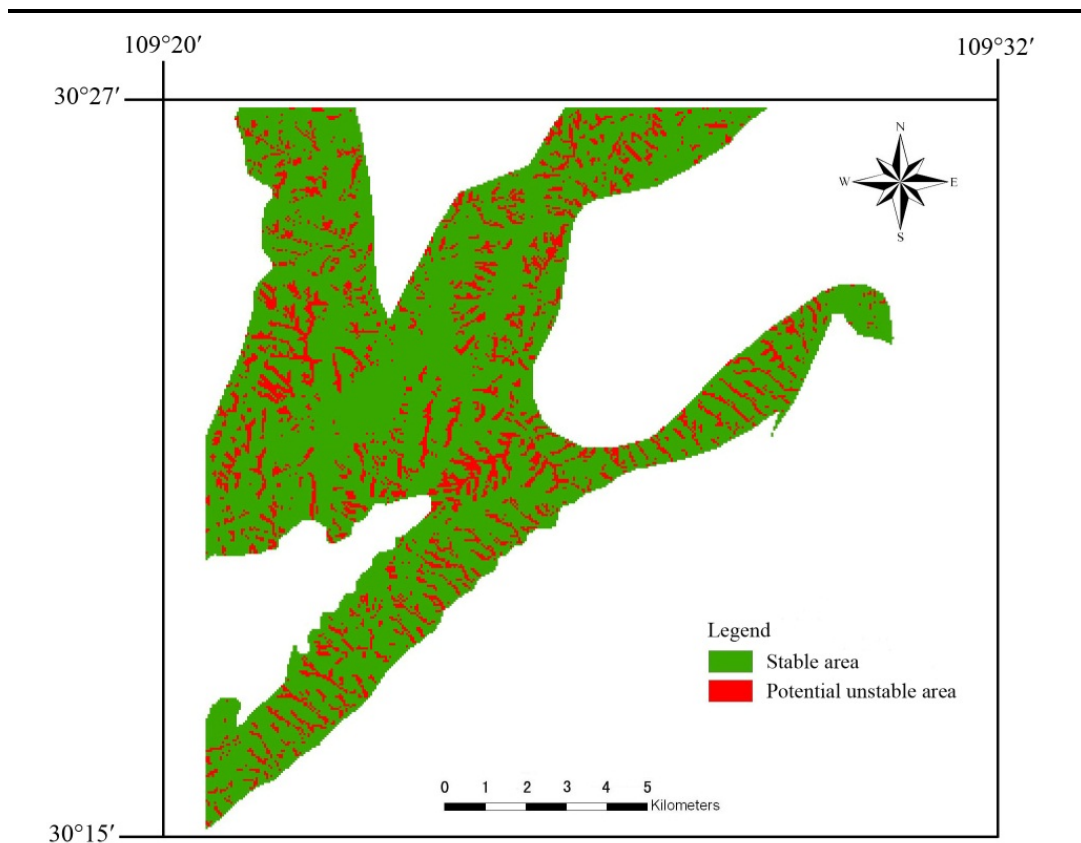

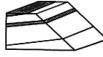



Fig.10



Table 1 Three different slope structures and the corresponding angle ranges

	angle (θ) range	
dip slope	$0^\circ < \theta < 20^\circ$; $340^\circ < \theta < 360^\circ$	
reverse slope	$160^\circ < \theta < 180^\circ$; $180^\circ < \theta < 200^\circ$	
skew slope	$20^\circ < \theta < 160^\circ$; $200^\circ < \theta < 340^\circ$	

" θ " is the angle between stratum dip direction and slope surface dip direction.



Table 2 Normalized sample data

Sample No	Road effect buffer	Slope angle	Slope structure type	Stream and gully effect buffer	Slope stability state	Sample No	Road effect buffer	Slope angle	Slope structure Type	Stream and gully effect buffer	Slope stability state
1	0.1	0.26	0.9	0.9	1	19	0.9	0.34	0.5	0.9	1
2	0.1	0.55	0.9	0.1	0	20	0.1	0.37	0.9	0.1	0
3	0.1	0.29	0.9	0.1	1	21	0.1	0.42	0.5	0.9	1
4	0.1	0.23	0.9	0.9	1	22	0.9	0.1	0.1	0.9	0
5	0.1	0.58	0.1	0.9	0	23	0.1	0.28	0.5	0.9	1
6	0.9	0.37	0.9	0.1	1	24	0.1	0.66	0.9	0.9	1
7	0.1	0.55	0.5	0.9	0	25	0.1	0.42	0.5	0.1	1
8	0.1	0.74	0.9	0.9	0	26	0.1	0.34	0.9	0.9	1
9	0.1	0.34	0.1	0.1	0	27	0.1	0.82	0.9	0.9	0
10	0.9	0.42	0.9	0.9	1	28	0.1	0.45	0.9	0.9	1
11	0.9	0.58	0.5	0.1	0	29	0.9	0.16	0.5	0.1	0
12	0.9	0.26	0.1	0.1	0	30	0.1	0.39	0.5	0.9	1
13	0.9	0.1	0.9	0.9	0	31	0.1	0.36	0.9	0.9	1
14	0.1	0.34	0.9	0.9	1	32	0.9	0.66	0.9	0.9	1
15	0.9	0.5	0.9	0.9	1	33	0.9	0.5	0.9	0.9	1
16	0.1	0.9	0.9	0.1	0	34	0.1	0.15	0.9	0.9	0
17	0.1	0.61	0.9	0.9	0	35	0.9	0.39	0.5	0.9	1
18	0.9	0.42	0.9	0.9	1						



Table 3 Predictive ability test result of the neural network

Sample number	Predicted Value	Actual Value	Absolute Error
26	0.99905	1	0.0009489
27	1.82e-06	0	-1.82e-06
28	2.2017e-005	1	0.99998
29	0.014818	0	-0.014818
30	0.99992	1	7.91e-05
31	0.99033	1	0.0096745
32	0.99999	1	5.56e-06
33	1	1	1.18e-09
34	1	0	-1
35	0.99754	1	0.0024614



Table 4 Comparison among the results of intelligent prediction, remote sensing and field investigation

Intelligent prediction results	Judgment by Remote sensing data	Judgment by field investigation